Dynamic simulation on the synthetic reservoir CERENA I

Compositional fluid flow simulation with 4D seismic monitoring on a reservoir with a large content of CO_2

Pinto, Pedro Tomás; Azevedo, Leonardo; Soares, Amílcar
Email addresses: pedrotmpinto@gmail.com; leonardo.azevedo@tecnico.ulisboa.pt; asoares@tecnico.ulisboa.pt
Centre for Petroleum Reservoir Modelling
Instituto Superior Técnico
Avenida Rovisco Pais, 1
1049-001 Lisboa

Abstract- This work focuses on the compositional fluid flow simulation of the synthetic reservoir CERENA-I, which mimics some characteristics of a Brazilian Pre-Salt field. This reservoir has a saturated oil leg with a retrograde condensation gas cap, both with a high content of CO_2, for which a production strategy capable of dealing with large quantities of gas was required and developed.
A rock physics model was also built for this reservoir in order to compute time-lapse seismic monitoring data with data retrieved from the compositional fluid flow simulation. This showed the influence of pore fluid changes in the seismic response of the reservoir.

Keywords: retrograde condensation gas, reservoir simulation, compositional fluid flow simulation, PVT analysis, CO_2, gas cycling, synthetic reservoir, seismic monitoring, AVO, time-lapse seismic

1. Introduction

The idea for this work came from a reservoir in the Brazilian Pre-Salt play (figure 1) with a very high content of CO_2. Due to its intrinsic characteristics this reservoir poses great challenges in every aspect of its production, from reservoir modelling and management, to surface facilities.
The reservoir covers an area of 567 km^2 about 300km offshore of Rio de Janeiro, in the Santos basin.

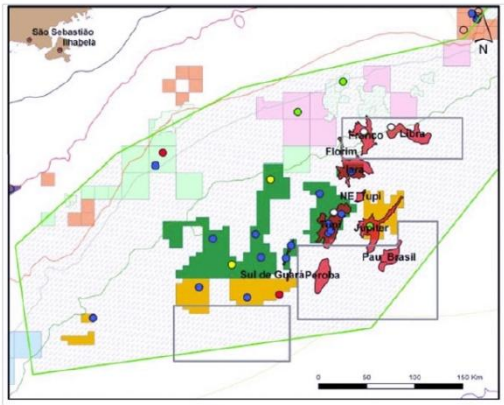

Figure 1: The Brazilian Pre-Salt play (Source: ANP).

It is situated in water depths of around 2000m, with the top of the reservoir situated at approximately 5200m. It has a 90m thick heavy oil leg with 18° API and 55% (molar) of CO_2 content. It also has a gas cap of retrograde condensation gas which contains approximately 80% (molar) of CO_2. [1]
CO_2 is one of the most infamous greenhouse gases and the ever increasing pressure to cut down its emissions will force the oil companies that wish to operate fields with conditions such as those found in this real oilfield to adopt strict environmental policies and practices.
In the Brazilian Pre-Salt Santos basin, Petrobras is currently undertaking a pilot CO_2 re-injection method to deal with the entire CO_2 produced in this basin, re-injecting it into Lula field in a WAG scheme (water-alternating-gas). This works both as a CO_2 storage method and also an Enhanced Oil Recovery method (EOR), since Lula contains only 8-12% of CO_2

content. This project aims to inject 2000 tonnes of CO_2 per day. [2]

Usually, CO_2 EOR processes are designed to optimize production while minimizing the amount of CO_2 necessary. Jessen et al, address the issue from an opposite perspective: how to use the greatest amount of CO_2 possible in an enhanced recovery mechanism. [3]

The initial objective for the project was to create a dynamic compositional model based on the CERENA-I data set, to test reservoir performance and fluid behaviour under such conditions as stated above, as well as production strategies. As the project matured, another idea started to be within reach: the link between compositional reservoir simulation and rock physics models, with the creation of a seismic data set to mimic a real time lapse seismic monitoring dataset.

2. The synthetic reservoir: CERENA-I

The CERENA-I model was created to replicate some characteristics of the Brazilian Pre-salt carbonate fields and it contains high-resolution data sets of petro-physical and petro-elastic properties. For the case study presented herein only the sets of porosity and permeability were used.

The model is composed of two facies: a reservoir facies, composed by microbiolites; and a non-reservoir facies composed by mudstones, on a corner-point grid with 161x161x300 cells, with 25x25x1m spacing. A porosity model was derived from the facies model recurring to stochastic sequential simulation[4](Figure 2).

It is clear that there are two different porosity distributions in the model: one with low values with high spatial continuity; and another with higher values and much more heterogeneous. These correspond to the facies already described. This effect is clearly interpreted on the marginal distribution of porosity for the entire model (Figure 3).

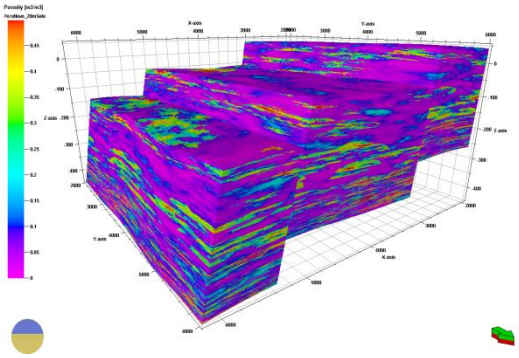

Figure 2: CERENA-I porosity model.

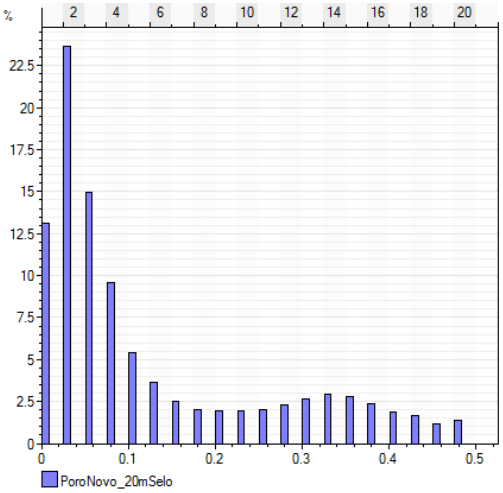

Figure 3: Histogram of porosity for both facies.

Permeability was modelled recurring to the porosity model and it exhibits a dependence that was derived from real analogues [5]. The joint distribution between both properties can be seen in Figure 4 [6].

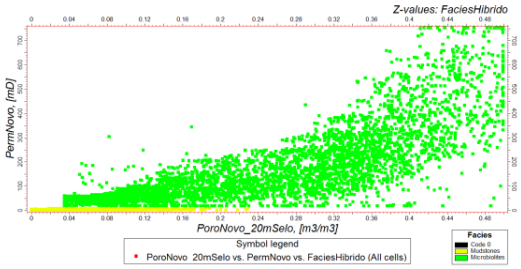

Figure 4: Joint distribution of porosity and permeability for both facies.

3. Dynamic simulation

Due to the lack of real data from analogue fields the oil composition for this study was obtained from a generic sample of oil from Petrel's® library, grouped to reduce

computation time and memory requirements, and with the molar percentages re-adjusted to the known CO_2 content of the analogue field (Table 1).

Table 1: Molar percentages of the oil with grouped components.

Component	Molar %	Mol. weight
CO_2	55.00	44.01
C_1	16.56	16.043
C_2	4.46	30.037
C_3	3.15	44.097
C_{4-6}	5.69	70.237
C_7^+	15.11	218

For this case study, the three parameter Peng-Robinson equation of state was chosen, and tuned to match the estimated PVT observations (Table 2).

Table 2: Estimated saturation pressures

Bubble point (bar)	Dew point (bar)
493	400

Since the final objective of this thesis was to produce time-lapse synthetic seismic volumes, the choice was made to run the simulation on a fine grid sectorial model (Figure 5) which, despite being considerably smaller, when compared to the original model, reproduces the total variability of the full field, instead of an up scaled model. This option was taken so that a dynamic model could be run and still maintain a high resolution in the final seismic models. From this point on, the link to the original full field model is severed and the study object is now the sectorial model. For this reason no boundary effects will be added to the dynamic model, to account for the influence of the remaining area.

The well pattern chosen for this study was a traditional five-spot configuration with four vertical producer wells in the corners and one vertical injector well in the centre (Figure 6).

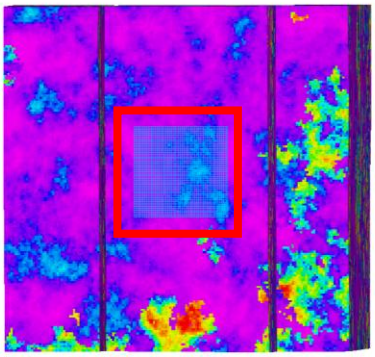

Figure 5: Sectorial model area.

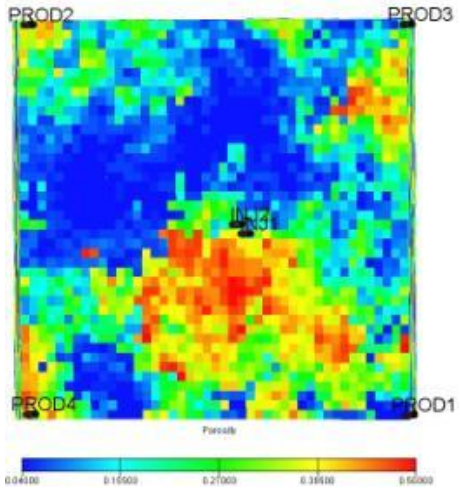

Figure 6: Well locations.

The model was initialized and the fluids in place(Table 3) were calculated for the equilibrium conditions (Figure 7).

Table 3: Fluids originally in place.

Reservoir volume of oil	Reservoir volume of gas
13.044802×10^6 rm^3	18.457536×10^6 rm^3

We first chose to produce the gas cap, to access its liquid condensate fraction. The fluid was condensed in surface separators and the resulting dry gas was re-injected back into the gas cap, to help keep reservoir pressure. The gas cap was produced for one year, after which the completions of the producer wells were closed in this zone and opened in the oil leg.

Figure 7: Reservoir section i=20, January 2014.

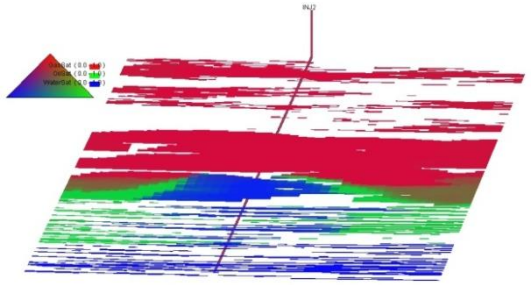

Figure 8: Reservoir section i=20, December 2025.

Observing the evolution of the dynamic properties within the reservoir grid (Figure 8), by 2025 it is possible to detect asymmetries in the evolution of the water displacement front, caused by heterogeneities in the reservoir.

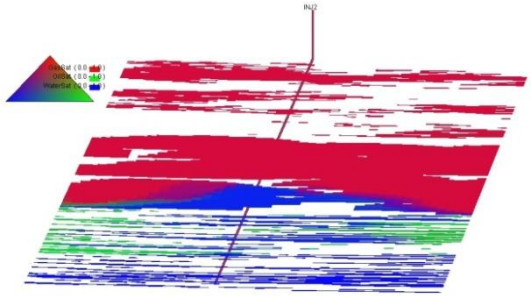

Figure 9: Reservoir section i=20, December 2045.

By the end of 2045 the top of the oil leg has been swept fairly efficiently while the lower part of the reservoir still shows oil pockets, showing the influence of reservoir heterogeneities and poor connectivity (Figure 9).

4. Production results

With the suggested production scheme, it was possible to obtain a stable nineteen year production plateau at 600 sm^3/day of oil, after which there is a five year period with a very slow increase of the water cut.

After the twenty four stable producing years, a considerable water breakthrough starts to happen and production starts to decline (figure 5).

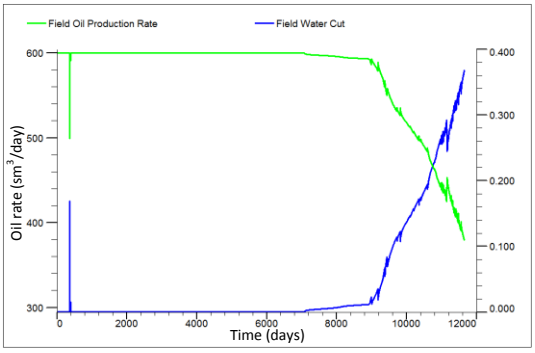

Figure 10: Oil production rate (green) and watercut (blue).

From the initial 13.04 million rm^3 of oil, a total of 6.7 million sm^3 were produced during the simulated 32 years simulated (Figure 11).

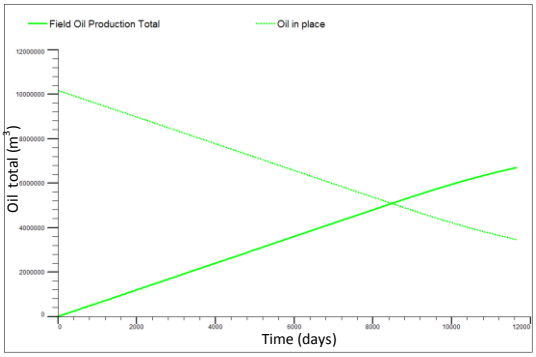

Figure 11: Total oil production and Oil in place.

Another important parameter to be analysed in this specific field is the evolution of the gas cycling performance. Figure 12 clearly shows that the gas production and re-injection rates and totals are equal throughout the production of the field so it was possible to implement a complete gas cycling scheme parallel to the oil production, therefore eliminating the need to export it. By the end of the simulation, the reservoir produced $2.08x10^{10}$ sm3 of gas (twenty billion standard cubic meters).

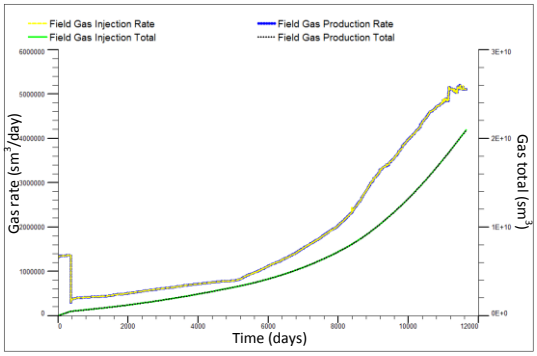

Figure 12: Field gas rates (upper) and gas totals (lower).

Taking a closer look at the performance of each individual well, particularly their oil production rates, we can conclude that reservoir heterogeneities substantially influence the performance of each well (Figure 13). The PROD4 well is the first to decline its production after nineteen years of production, causing the slight decline in field production mentioned earlier. Twenty four years into production the PROD1 well declines drastically, starting the decline in the overall field production as later wells PROD3 and PROD2 also decline.

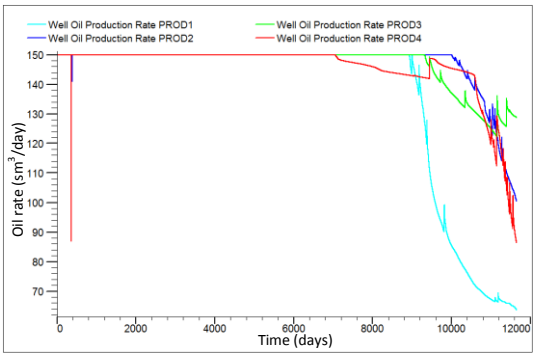

Figure 13: Well oil production rates.

Figure 14 contains the evolution of the bottom hole pressures for the four producer wells. It is evident that each well has a distinct behaviour, having different changes in pressure over time. One interesting detail in this evolution is that there is a clear difference between the gas cap and the oil leg production. The well PROD3, for instance, required the highest pressure drop to produce the desired flow in the gas cap, while on the oil leg it was the opposite. We can also see that this well has a very constant bottom hole pressure throughout the production, whilst the other three present significant changes.

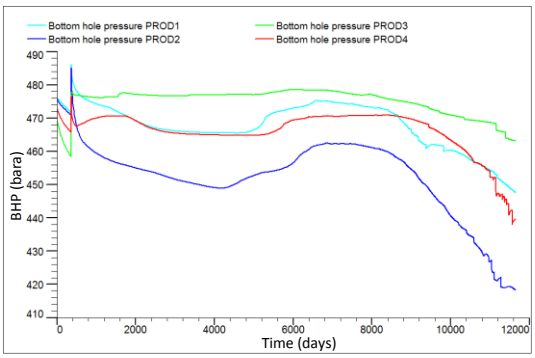

Figure 14: Well bottom hole pressures.

Table 4 gathers the total fluids produced and injected in the reservoir.

Table 4: Total fluids produced and injected (metric units).

	Gas cap	Oil leg
Produced oil (sm^3)	$2.16x10^5$	$6.48x10^6$
Produced gas (sm^3)	$4.95x10^8$	$2.04x10^{10}$
Re-injected gas (sm^3)	$4.95x10^8$	$2.04x10^{10}$
Produced water (sm^3)	1.35	$2.9x10^5$
Injected water (sm^3)	-	$4.63x10^6$

5. Seismic monitoring

This part of the work explores the advantages of the compositional fluid flow simulation to model the changes in the seismic response of the reservoir during production. Once the compositional fluid flow simulation was run and optimized, the data regarding fluid saturation, density and compressibility from simulated time steps were gathered.

A rock physics model was created for specific time steps and a set of synthetic time-lapse seismic data was then computed for each. The changes in seismic response were observed by subtracting the seismic volumes. To enhance the influence of pore fluids on the seismic response of the reservoir, seismic attributes such as the Lamé parameters were calculated and revealed distinct trends for each fluid type.

5.1. Rock physics model

The first step towards the generation of seismic data was to create a rock physics model according to the Xu&Payne[7] methodology. The mineral matrix elastic properties were modelled using the Voigt-Reuss-Hill average of the minerals present. For the reservoir facies, the Lagoa Salgada's stromatolites composition[8] was used. The Mudstone facies was assumed to be composed by Calcite. Table 5 contains mineral matrix elastic moduli for both facies.

Table 5: Elastic moduli for both facies.

Facies	K(GPa)	μ(GPa)
Reservoir	69.198	33.368
Mudstones	76.8	32

The closed micro-porosity was modelled with a Differential Effective Medium[9] and the output was used for the Dry Rock model calculation.
Not having enough real data to produce a rock physics set based on contact models, a simpler approach was taken and a Hashin-Shtrikman theoretical bounds model[9] was calculated (figure 15) to model the macro-porosity.

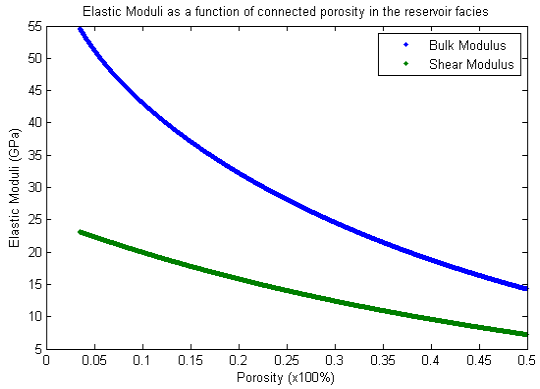

Figure 15: Rock physics model for the dry connected porosity in the reservoir facies.

Several simulated time steps were chosen and the data retrieved from the compositional simulation, regarding fluid compressibility, saturations and densities was used to create time lapse models of, respectively, elastic moduli and density for the reservoir facies[1]. Table 6 contains the selected time steps.

Table 6: Selected time steps for the seismic monitoring.

Step zero	01-January-2014
Step one	01-January-2015
Step two	01-January-2021
Step three	01-December-2027
Step four	01-December-2033
Step five	01-December-2039
Step six	01-December-2045

The density models were calculated with a simple weighted average of fluid saturations and densities, while the Bulk modulus models were calculates using Gassmann's relation[10](equation 1).

$$\frac{K_{sat}}{K_0 - K_{sat}} = \frac{K_d}{K_0 - K_d} + \frac{K_{fl}}{\emptyset\left(K_0 - K_{fl}\right)}$$

Equation 1: Gassmann's relation.

Having the time-lapse volumes of elastic moduli it was possible to calculate Vp and Vs models for each time step, which were later used to compute synthetic seismic.

5.2. Synthetic seismic volumes

Shuey's approximation of the Zoeppritz equation[11] was used to calculate angle-dependent reflection coefficients for twenty five angles of incidence (from 0 to 45 degrees). For each offset angle, a specific wavelet was provided and, using a convolutional forward model, seismic amplitudes were calculated for each cell.
The seismic volumes were then divided in three groups and stacked: a near-stack (figure 16), with offsets from 0^o to 16.2^o; a mid-stack, with offsets from 14.4^o to 30.6^o; and a far-stack, with offsets from 28.8^o to 45^o. A full-stack volume was also created as an average of all offsets.

[1] This is due to the fact that flow was not simulated in the mudstones facies.

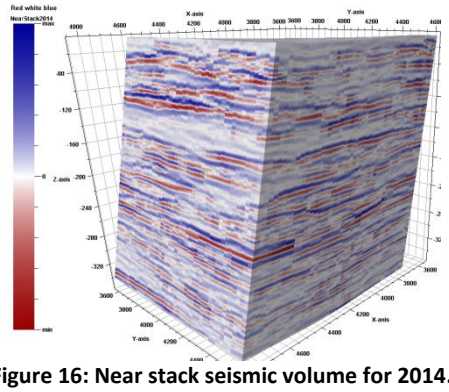

Figure 16: Near stack seismic volume for 2014.

The initial seismic volume was subtracted to each time-lapse seismic volume and the results showed the influence of the production strategy on the seismic response of the reservoir. By the end of the first year, with the gas cap under natural depletion with gas re-injection, a difference occurs at the gas-oil contact and around the re-injection well (figure 17).

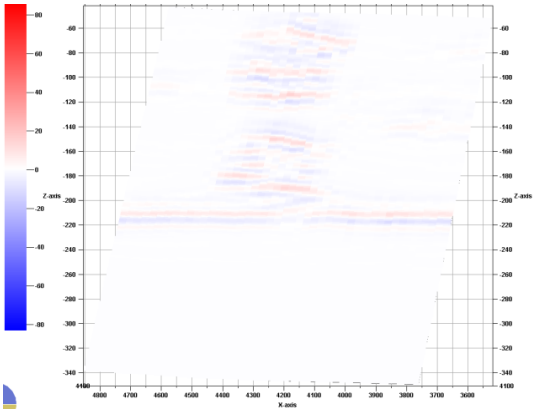

Figure 17: Amplitude differences for 2015.

Water injection starts in the oil leg as soon as this zone is produced, in 2015. By 2021, the effect of water injection can be seen (figure 18) as a contrast in the seismic amplitudes in the surroundings of the water injection well.

With the continuous water injection throughout the remaining life of the field, the contrast induced by the water spreads out as oil is swept (figure 19). The gas cap also exhibits an increasing contrast, as gas is re-injected into it and is compressed.

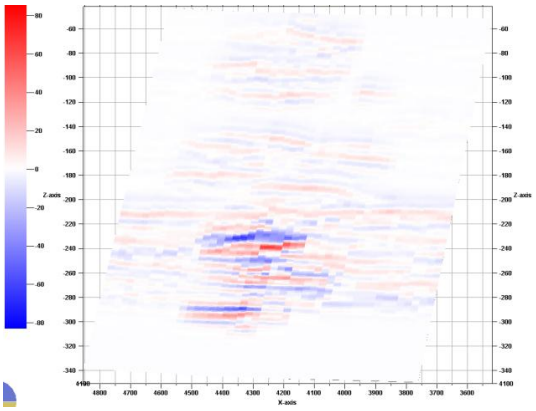

Figure 18: Amplitude differences for 2021.

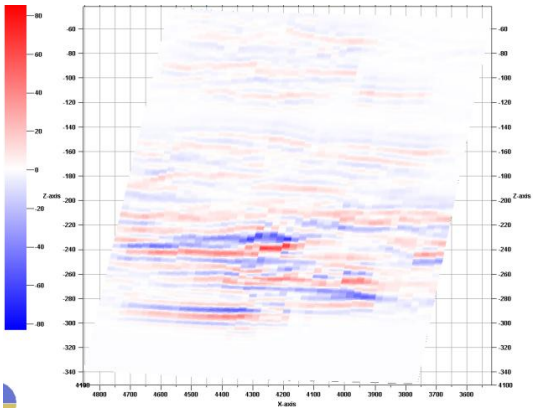

Figure 19: Amplitude differences for 2039.

5.3. Seismic attributes

For a better understanding of the seismic response of reservoir rocks containing different fluids, some seismic attributes such as the Lamé parameters (equations 2 and 3) were calculated and analyzed.

Figure 20 corresponds to a plot of **μ** as a function of **λ,** where it can be seen that there are three distinct trends of Lamé parameters: the Mudstones trend, reaching higher **λ** values with a narrower **μ** window; and two similar trends with a wider range of **μ** values.

$$\mu = \rho Vs^2$$ **Equation 2: μ Lamé parameter.**

$$\lambda = \rho Vp^2 - 2Vs^2$$ **Equation 3: λ Lamé parameter.**

These two trends correspond to the aquifer trend (on the right) and the hydrocarbons trend (on the left). Taking a closer look it becomes clear that the hydrocarbons trend actually corresponds

to another two very close trends: one on the left corresponding to the gas trend; and one on the right which corresponds to the oil trend.

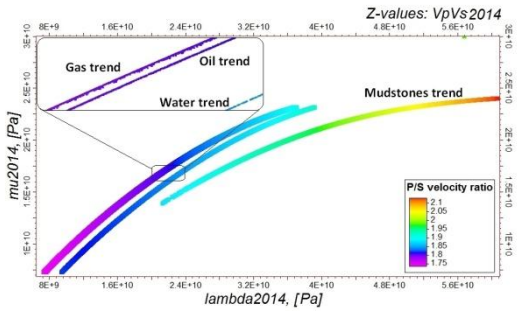

Figure 20: Lamé parameters trends.

Calculating volumes of differences in seismic attributes it becomes clear that the migration of cells from one trend to another is not as straightforward as it appeared. The cells that present an increase in **λ** (Figure 21, red box) correspond to the surroundings of the gas re-injection well, where gas is compressed and acquires a stiffer seismic response, and also to the producer wells on the corners, where the liquid condensation due to the production drawdown induces a stiffer response (Figure 22).

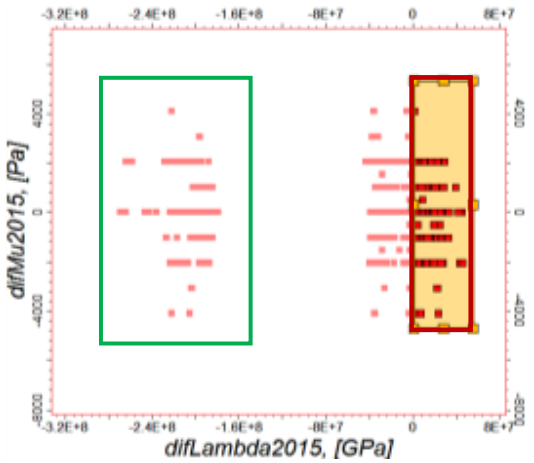

Figure 21: Changes in λ from 2014 to 2015.

The group of cells which present the greatest decrease in **λ** (Figure 21, green box) corresponds to the top of the oil leg, where the pressure drop leads to the crossing of the bubble point and the appearance of gas (Figure 23).

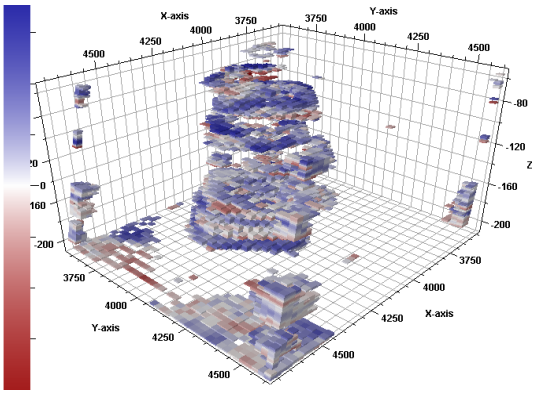

Figure 22: Effect of reservoir production on the seismic model.

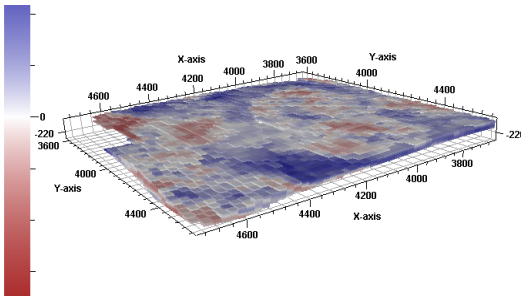

Figure 23: Effect of the gas-oil contact on the seismic model.

Figure 24 shows another interesting effect of the production of the reservoir in its seismic trends.

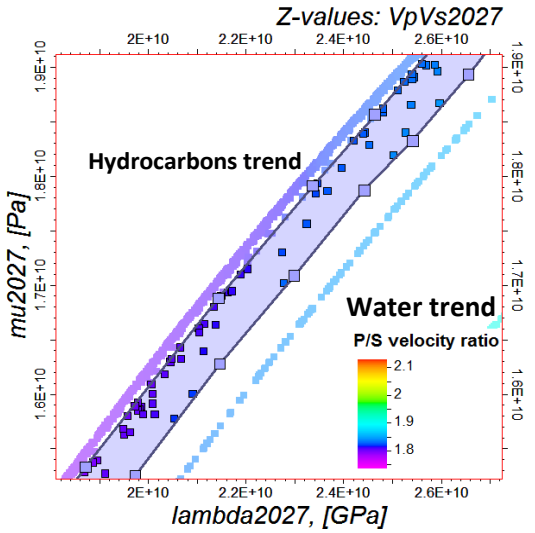

Figure 24: Migration of cells from the hydrocarbons trend to the oil trend.

As water is injected into the reservoir and sweeps away the oil, the swept cells start moving towards the water trend. Applying an inclusive filter for these cells to the seismic volume it is possible to identify the

swept cells (figure 25) and assess the performance of the water injection.

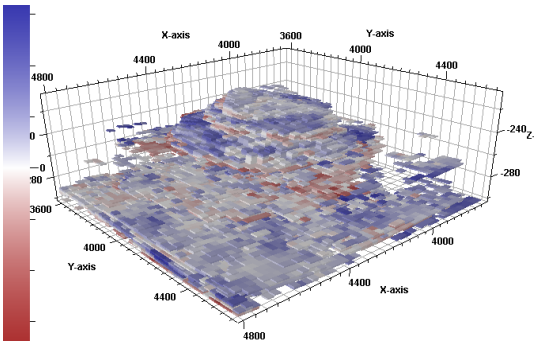

Figure 25: Effect of water injection on the seismic model.

6. Conclusions

The CERENA-I static model was used as a starting point for the construction of a dynamic model to reproduce some specific conditions of a Brazilian pre salt reservoir, and to test reservoir performance and production strategies.

The reservoir was produced for thirty two years, from January 2014 to December 2045. The liquid fraction of the gas cap allowed a total production of 2.16×10^5 sm^3 of oil by the end of the first year of production while the oil leg was produced for thirty one years, with a steady production plateau of eighteen years, reaching a total of 6.48×10^6 sm^3 of oil.

The presence of a free gas zone associated with an oil leg indicates that the oil is saturated, or at equilibrium. This implies that any drop in the oil pressure will result in the exsolution of gas. For the oil to flow, a drawdown in the wells is required and in this type of reservoir it is impossible for it to happen without producing very large amounts of gas. The production strategy proved to be able to handle the large quantities of gas produced with little impact in the oil production. This was reached through an efficient gas cycling loop, which was implemented by re-injecting the gas in the centre of the gas cap.

As a final remark on reservoir management, we can see the presence of high amounts of CO_2 in this reservoir as both a problem and an advantage: on the one hand the reservoir will produce large quantities of this gas which will have to be dealt with, increasing surface facilities complexity and production costs; on the other hand the reservoir benefits from a natural enhanced recovery mechanism, as the high content of dissolved CO_2 produces a low viscosity fluid, which greatly facilitates production and increases recovery.

What started as the main objective of this thesis, the construction of a compositional dynamic model, gradually became a tool for the construction of a time lapse seismic data set, as the potential of compositional fluid flow simulation for detailed rock physics modelling was perceived. This rock physics model was then used to compute 4D seismic data which was analysed to assess the influence of changes in pore fluids on the seismic response of the model.

The compositional model allowed a detailed tracking of the evolution of pore fluid compressibility and density for each cell. This, together with a rock physics model for the reservoir matrix, was used to compute a synthetic seismic monitoring campaign. Unlike unconsolidated sandstone reservoirs, carbonates have high elastic moduli and their overall seismic response tends to be little affected by changes in pore fluid properties. Nevertheless, changes in the seismic response of this reservoir were observed, and directly correlated to the production strategy employed.

The AVO analysis did not prove to be of relevance in the seismic monitoring campaign as practically no changes occur in the AVO properties throughout the production of this field. On the contrary, the Lamé parameters showed a clear separation of fluid trends and allowed a direct correlation between the production strategy and the changes in the seismic response of the reservoir, proving in this case to be a good reservoir monitoring tool.

By the end of the first year of production, with the reservoir under natural depletion

with gas cycling, the pressure drop led to an increase in gas saturation just under the gas-oil contact, which was manifested in the seismic response as a reduction in the λ parameter. At the same time the re-injected gas created an area around the re-injection well which showed an increase in the λ parameter, caused by the gas acquiring a stiffer behaviour due to compression.

The production of the oil leg also has a visible impact on the seismic response, as the injected water sweeps the oil and induces a stiffer seismic response with swept cells travelling from the oil to the water seismic trend.

Finally, another interesting fact can also be pointed out from this work, and it relates to seismic inversion, in which usually static reservoir properties are inferred from seismic amplitudes. Reservoirs are dynamic systems and, as demonstrated in the previous section, fluid density and saturation can have a direct impact on the seismic response of a reservoir. For this reason, care must be taken when producing inverse models, so as to not interpret seismic amplitudes solely as the influence of static properties when in fact dynamic properties can also play an important role.

7. References

[1] ANP (2010), Exame e avaliação de dez descobertas e prospectos seleccionadas no Play do Pré-Sal em águas profundas na bacia de Santos, Brasil, Rio de Janeiro - Brasil, Gaffney, Cline & Associates.

[2] Araújo, C. (2013). CO2 injection in Carbonate Reservoirs in Brazil. *Petrobras/CENPES.*

[3] Jessen, K., Sam-Olibale, L., Kovscek, A., & Orr, F. (s.d.). Increasing CO2 storage in oil recovery. *Department of Petroleum Engineering, Stanford University*.

[4] Soares, A. (2001). Direct Sequential Simulation and Co-simulation. *Mathematical Geology*.

[5] Kansas Geological Survey (2004). *Sedimentologic and Diagenetic Characteristics of the Arbuckle Group.*

[6] Horta, A., & Soares, A. (2010). Direct Sequential Co-Simulation with Joint Probability Distributions. *Mathematical Geosciences*.

[7] Xu, S., & Payne, M. (2009). Modeling elastic properties in carbonate rocks. *The Leading Edge*, pp. 66-74.

[8] Archilha, N., Missagia, R., Ceia, M., & Neto, I. (2013). Petrophysical, mineralogical and elastic property characterization of Halocene carbonates from Salgada lagoon, Brazil. *SBGf*.

[9] Mavko, G., Mukerji, T., & Dvorkin, J. (2009). *The Rock Physics Handbook.* Cambridge University Press.

[10] Smith, T., Sondergeld, C., & Rai, C. (2003). Gassmann fluid substitution: A tutorial. *Geophysics*, pp. 430-440.

[11] Avseth, P., Mukerji, T., & Mavko, G. (2005). *Quantitative Seismic Interpretation.* Cambridge University Press.